ISSN:(O)2320-5407, ISSN(P)3107-4928 Int. J. Adv. Res. 14(08), August-2026, 237-248

ISSN (O): 2320-5407
ISSN (P): 3107-4928

Journal Homepage: -www.journalijar.com

INTERNATIONAL JOURNAL OF ADVANCED RESEARCH (IJAR)

Article DOI:10.21474/IJAR01/23956
DOI URL: http://dx.doi.org/10.21474/IJAR01/23956

RESEARCH ARTICLE

BRIDGING CONVENTIONAL AND INTELLIGENT MPPT TECHNIQUES: A HYBRID ANN-P&O APPROACH FOR SMART PHOTOVOLTAIC SYSTEMS

Sada Traore, Ndeye Adjaratou Diop, Ansoumane Diedhiou and Moustapha Thiame

Manuscript Info

Manuscript History
Received: 8 June 2026
Final Accepted: 10 July 2026
Published: August 2026

Key words:-
photovoltaic systems; maximum power point tracking; artificial neural network; perturb and observe; hybrid control; buck converter.

Abstract

This study investigates maximum power point tracking (MPPT) for a 250.27 W photovoltaic module connected to a buck converter. The proposed strategy combines an artificial neural network (ANN), which estimates the maximum-power-point voltage from irradiance and temperature, with a local perturb-and-observe (P&O) correction. The ANN rapidly repositions the voltage reference after an environmental change, while the hybrid P&O stage refines that reference using a small, bounded correction. Discrete simulations at 20 kHz are performed under a stepped irradiance profile of 1000, 600, 800, 400, and 1000 W/m² at 25 °C. Under the nominal PV model, conventional P&O exhibits power ripple of up to 44.23 W and response times exceeding 100 ms during some transitions, whereas the ANN and hybrid controllers respond within a few microseconds. The demonstrate d result is that the hybrid controller preserves the rapid nominal response of the ANN and substantially reduces ripple relative to conventional P&O. However, because the ANN was trained using the same nominal PV model, the hybrid and standalone ANN responses nearly overlap; consequently, these nominal simulations do not demonstrate a robustness advantage of the hybrid controller over standalone ANN. An out-of-model robustness test, based on parameter mismatch without ANN retraining, is therefore identified as future work to quantify the specific contribution of P&O refinement.

Introduction: -

Maximum power point tracking is required because the current–voltage and power–voltage characteristics of a photovoltaic system vary with irradiance and cell temperature [1], [2]. Conventional techniques remain attractive because of their implementation simplicity [3], whereas data-driven controllers can directly infer an operating reference from measured environmental variables [4]. Comparisons of MPPT methods highlight a trade-off among speed, accuracy, and complexity [3], [5], which motivates hybrid strategies [9], [10]. Under the dynamic profile investigated here, conventional P&O requires more than 100 ms to settle after the 800→400 W/m² transition, with residual ripple close to 24 W; this observation is consistent with the perturbation-step/ripple trade-off described for P&O [6].Recent studies have evaluated ANN training algorithms for PV energy harvesting and hybrid intelligent–conventional MPPT structures, including ANN-assisted and ANN–P&O approaches under changing or partially shaded conditions [11]– [13].

Corresponding Author: -Sada Traore

P&O is widely used in low-cost PV converters [3], [7]. Its main limitation is the persistent perturbation around the MPP, which produces steady-state power ripple and can delay tracking under rapidly changing irradiance [6], [7]. An ANN can estimate the MPP operating voltage from irradiance and temperature [4]. Its accuracy, however, depends on the representativeness of the training data and on the mismatch between the model used for learning and the system being controlled. Studies of hybrid strategies indicate the value of combining global search or intelligent estimation with local refinement, particularly under partial shading [8]– [10].These recent contributions further show that comparisons must report separately the estimator accuracy, transient convergence, steady-state ripple, and energy-based tracking efficiency [11]– [13].

This work proposes an interpretable ANN–P&O hybrid architecture compatible with a voltage-control loop. Its contributions are: (i) an ANN trained using G and T to produce Vmp, Imp, and Pmp, with V_{mp} used as the reference; (ii) P&O refinement applied to the voltage reference rather than direct mixing of duty cycles; (iii) a dynamic comparison with conventional P&O using the same converter and G(t) profile; and (iv) an explicit analysis of the limitations arising from ANN training on the nominal PV model.

Photovoltaic System Modeling: -
Electrical Model of the Photovoltaic Module: -
✓ Single-Diode Electrical Model: -

To simulate the electrical behavior of a photovoltaic module under variable environmental conditions, a model relating the physical panel parameters to irradiance G and temperature T is required. The single-diode model is widely used for this purpose because it provides a useful compromise between accuracy and simplicity [1], [2].

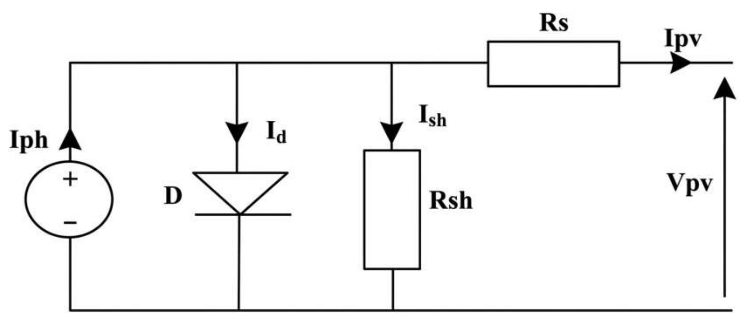

Figure 1. Equivalent circuit of a solar cell

✓ Characteristic Equation of a Photovoltaic Panel: -
The current–voltage (I–V) behavior of a PV generator is described by the following equation: -

$$I = I_{ph} - I_s\left(\exp\left(\frac{q(V + R_s I)}{nkT}\right) - 1\right) - \frac{V + R_s I}{R_{sh}} \quad (1)$$

I and V are the module output current (A) and terminal voltage (V), respectively; I_{ph} is the photocurrent, which depends on irradiance and temperature; $I_s$is the reverse diode saturation current; R_s and R_{sh} are the series and shunt resistances (Ω), respectively; q is the elementary charge (1.6×10^{-19} C), k is the Boltzmann constant (1.38×10^{-23} J/K), and n is the diode ideality factor (typically between 1 and 2).

Influence of irradiance and temperature: -
• Photocurrent: -

The photocurrent I_{ph} varies almost linearly with solar irradiance G, which directly increases the short-circuit current and the maximum power of the PV module. The effect of temperature on Iph remains limited and only weakly affects the operating point.

$$I_{ph} = \left[I_{sc\_ref} + \alpha_{Isc}(T - T_{ref})\right] \cdot \frac{G}{G_{ref}} \quad (2)$$

I_{sc_ref} is the short-circuit current at the reference temperature T_{ref}; α_{Isc}: is the short-circuit-current temperature coefficient (A/K);G is the instantaneous irradiance (W/m²) and$G_{ref}$is the reference irradiance (1000 W/m²).

• **Reverse saturation current I_s**

The reverse saturation current I_s increases exponentially with temperature, causing a reduction in open-circuit voltage V_{oc} and a shift of the maximum power point toward lower voltages. Thus, temperature mainly affects the voltage component of the PV generator, whereas irradiance primarily affects the current component.

The reverse saturation current is expressed as: -

$$I_s = I_{s0}\left(\frac{T}{T_{ref}}\right)^3 \cdot \exp\left[\frac{qE_g}{nk}\left(\frac{1}{T_{ref}} - \frac{1}{T}\right)\right] \qquad (3)$$

I_{s0}: saturation current at T_{ref}

Eg: material bandgap energy (Si: approximately 1.12 eV)

I–V and P–V characteristics: -

The performance of a photovoltaic module is mainly analyzed through it's I–V and P–V characteristics. The I–V curve describes the relationship between panel current and voltage, whereas the P–V curve represents delivered power as a function of voltage. The power produced by the PV panel is given by: P=V×I On the P–V curve, the maximum power point (MPP) is the maximum power that the panel can deliver for a given irradiance and temperature. This point is characterized by a voltage V_{MPP} and a current I_{MPP}. The main objective of an MPPT algorithm is to force photovoltaic-system operation around this point in order to maximize the extracted energy.

DC–DC converter and power interface: -

Buck converter: -

The Buck converter is a step-down DC–DC converter that adapts the PV generator voltage to the load by controlling the duty cycle, as illustrated in Figure 2. It relies on high-frequency switching of an electronic switch together with an inductor and a capacitor to provide a regulated output voltage.

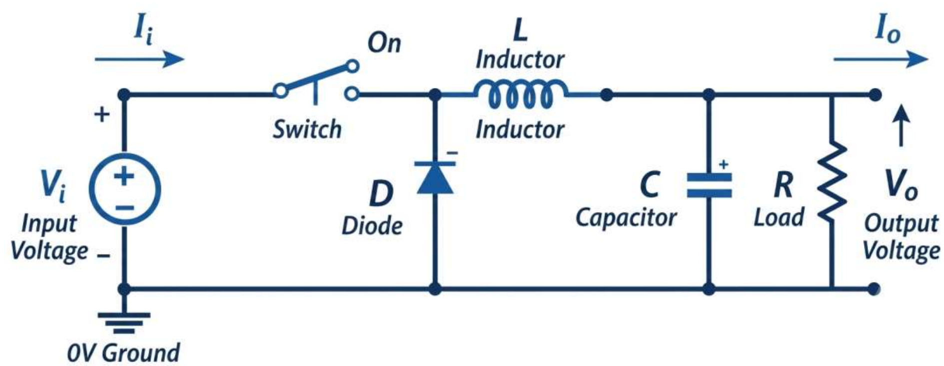

Figure 2. Schematic diagram of a Buck converter

Operating principle:-

The Buck converter operates through PWM switching of the electronic switch, alternating between conduction and blocking intervals to transfer and release energy to the load. In continuous-conduction mode, this operation is described by two sets of differential equations corresponding to the ON and OFF switch states, given by Eqs. (4) and (5), respectively.

Mathematical modeling:-

In continuous-conduction mode, the Buck converter is described by the inductor and capacitor equations. The electrical simulation includes an inductor, an input capacitor, an output capacitor, a diode, and a MOSFET switched at 20 kHz. The power-stage parameters are listed in Table 4.

When the switch is closed (ON):

$$\begin{cases} \dfrac{\mathrm{d}i_L(t)}{\mathrm{d}t} = \dfrac{V_{in} - V_{out}}{L} \\ \dfrac{\mathrm{d}V_{out}(t)}{\mathrm{d}t} = \dfrac{i_L(t) - V_{out}(t)/R}{C} \end{cases} t \in [0, \alpha T] \quad (4)$$

When the switch is open (OFF):

$$\begin{cases} \dfrac{\mathrm{d}i_L(t)}{\mathrm{d}t} = \dfrac{-V_{out}}{L} \\ \dfrac{\mathrm{d}V_{out}(t)}{\mathrm{d}t} = \dfrac{i_L(t) - V_{out}(t)/R}{C} \end{cases} t \in [\alpha T, T] \quad (5)$$

These equations are implemented in Simulink using logical subsystems (or Switch blocks) controlled by a PWM signal.
A Buck converter is a step-down DC–DC converter that produces an output voltage lower than the input voltage. Its conversion ratio depends directly on the switch ON time.

This ratio is called the duty cycle, denoted D, and is defined as: -

$$D = \frac{V_{out}}{V_{in}} \quad (6)$$

where Vin is the input voltage and Vout is the output voltage.

By definition, the duty cycle is the ratio of the ON time (t_{on}) to the switching period T and is bounded between 0 and 1. The expressions for the output-current, inductance L, and capacitance C are given in Eqs. (7) and (8), respectively.

$$I_{out} = \frac{P_{mp}}{V_{out}} \quad (7)$$

$$L = \frac{(V_{in} - V_{out}) \cdot D}{\Delta_{IL} \cdot f_s} etC = \frac{I_{mp} \cdot D}{\Delta v_0 \cdot f_{sw}} \quad (8)$$

For dimensional consistency, all temperatures used in Eqs. (2) and (3) are expressed in kelvin, qEg/(nkT) is dimensionless, and the exponential argument in Eq. (1) is dimensionless. In the Buck-converter equations, dIL/dt has units of A/s and dVout/dt has units of V/s. Equations (7) and (8) yield Iout in amperes, L in henries, and C in farads when SI units are used. Subscripts and symbols are retained consistently throughout: Vpv and Ipv denote PV-side variables, whereas Vout and Iout denote load-side variables.

Electrical parameters of the Jinko Solar PV 250W PV module: -
The electrical parameters used in the simulation are summarized in Table 1. They correspond to the Jinko Solar 250 W module selected in the PV Array block. This table presents the electrical parameters actually used for the PV module and the single-diode model.

Table 1: Electrical parameters of the Jinko Solar 250 W module used in the PV model

Parameter	Values
Maximum power P_{max}	250.27 W
Open-circuit voltageV_{oc}	35.8 V
Short-circuit current Isc	9.32 A
Voltage at maximum power pointV_{mp}	29.0 V
Current at maximum power pointI_{mp}	8.63 A
Light-generated currentIL	9.3424 A
Temperature coefficient ofI_{sc}	0.041996 %/°C
Temperature coefficient ofV_{oc}	−0.333 %/°C
Number of cells in series	60

Overview of conventional MPPT algorithms: -
MPPT modifies the apparent impedance seen by the PV generator to maintain operation near the MPP. Table 2 presents the common methods; P&O is selected as the conventional reference method because it is simple to implement but sensitive to the speed–ripple trade-off. The operating point is shifted by changing the converter duty cycle. In the Buck converter studied here, this action is produced indirectly by the Vpv control loop. Table 2 places P&O and the main alternatives in the MPPT literature.

Table 2: Comparison of the Main MPPT Methods

Algorithm	Principle	Advantages	Limitations
Perturb and Observe (P&O) [3], [6]	Perturbs the operating point and observes the power change by adjusting the duty cycle.	Simple, low cost	Oscillates around the MPP; sensitive to rapid variations.
Incremental Conductance (IncCond) [3], [5]	Compares instantaneous and incremental conductance to locate the MPP.	More accurate under rapid variations	More complex than P&O.
Fractional Open-Circuit Voltage [3], [5]	Estimates the MPP voltage from the open-circuit voltage.	Simple; few measurements	Lower accuracy; requires periodic open-circuit measurement.
Fractional Short-Circuit Current [3]	Estimates the MPP current from the short-circuit current.	Simple implementation	Power losses during short-circuit measurement.
Optimized methods (Fuzzy, Neural, PSO) [4], [9]	Use artificial intelligence or heuristic optimization.	Potentially high tracking performance	Higher computational burden and tuning effort.

In this study, the P&O algorithm was selected for its simplicity and effectiveness.

Perturb and Observe (P&O) Method: -
The conventional P&O algorithm measures $P_{pv} = V_{pv} \times I_{pv}$, calculates the power variation between two instants, and then increases or decreases the duty cycle according to the sign of that variation. The settings used here are Ts,P&O = 1 ms, ΔD = 0.002, and D0 = 0.82.

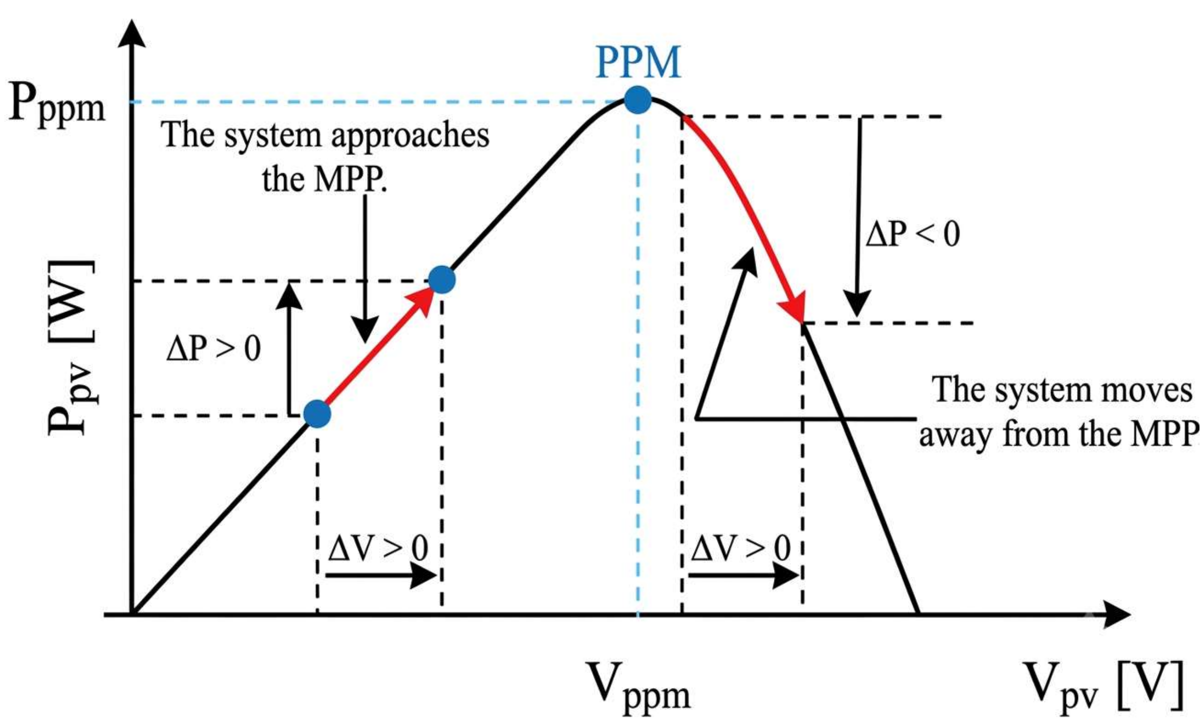

Figure 3. Maximum power point search using the P&O method [3], [6].

Despite its advantages, P&O has notable limitations, including permanent oscillations around the MPP at steady state and poor performance under rapid irradiance variations.

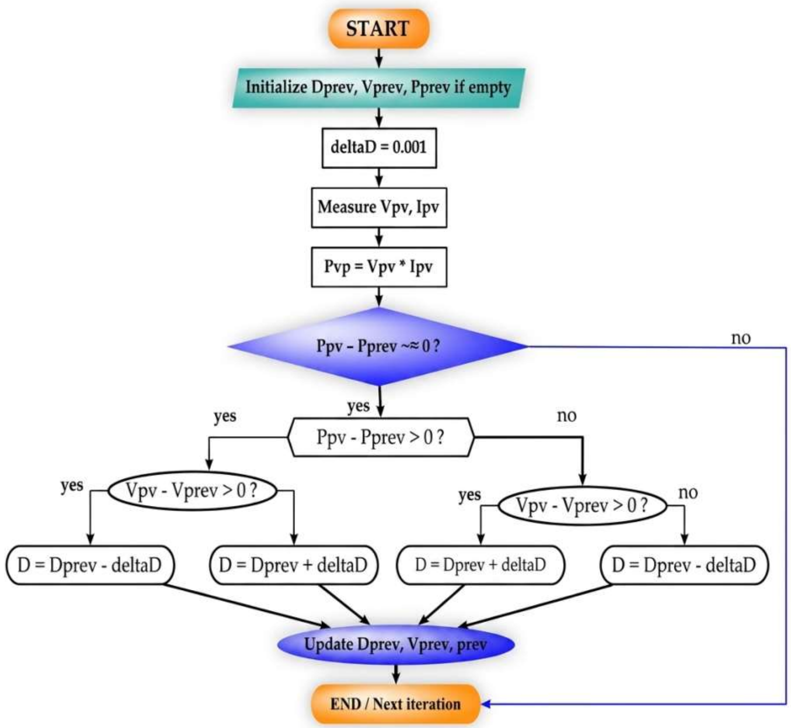

Figure 4. Flowchart of the P&O algorithm for a PV system

Hybrid ANN–P&O MPPT: -

An artificial neural network (ANN) is used as a static MPP estimator. It does not replace the converter; it provides a reference input to the control loop. Its quality depends on the operating range covered by the training data. In this study, the ANN receives irradiance G (W/m²) and temperature T (°C). It produces V_{mp}, I_{mp}, and P_{mp}; only V_{mp} is used as the V_{ANN} reference. The MLP network has two hidden layers with 32 and 16 neurons and three outputs, and it was trained using data from the nominal PV model.

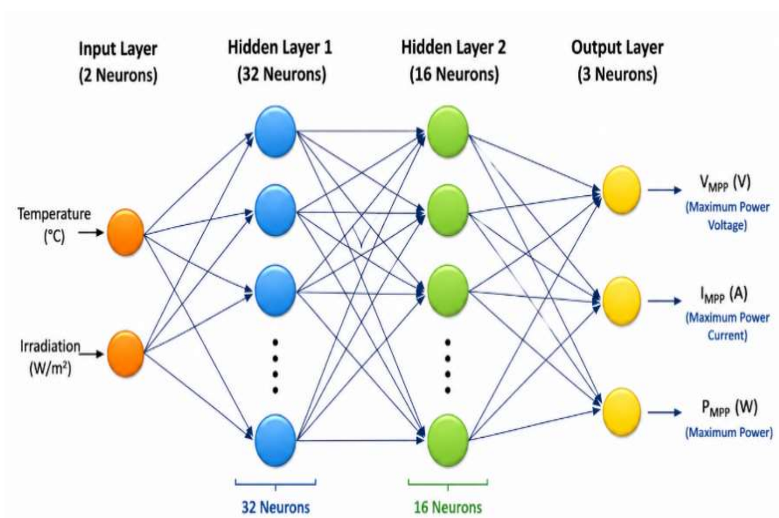

Figure 5. ANN architecture diagram 5.

Hybrid Ann- P&O: -

Overall system architecture: -

The architecture proposed in Figure 6 combines a photovoltaic generator, a Buck DC–DC converter, an equivalent resistive load, and a hybrid ANN–P&O MPPT controller.

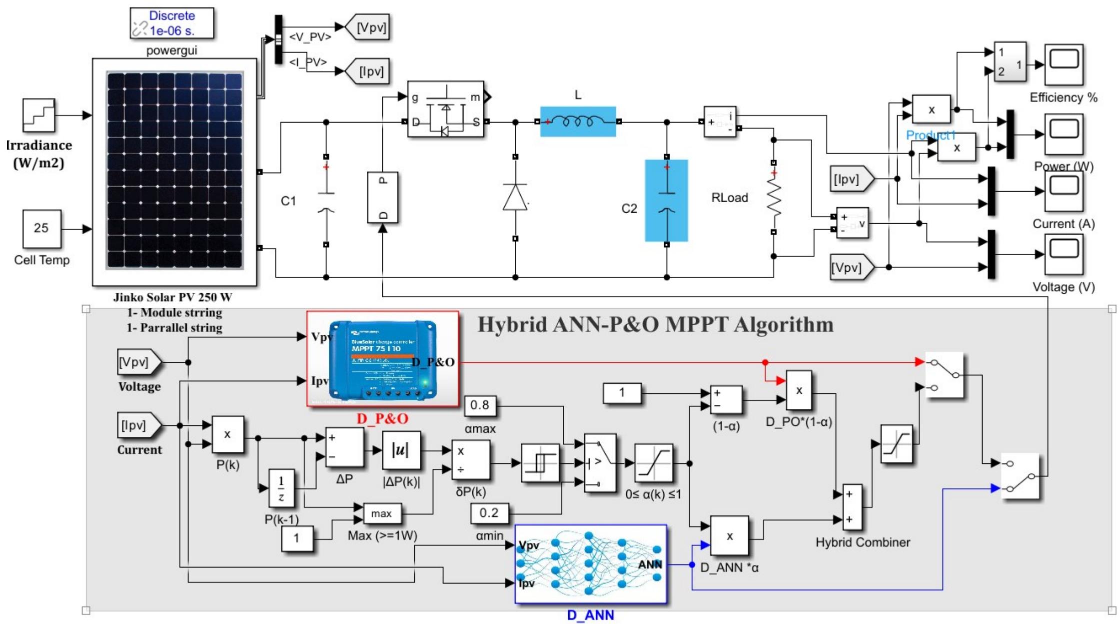

Figure 6. Photovoltaic system with hybrid ANN–P&O MPPT control

The photovoltaic generator is modeled using a single-diode model whose behavior depends on solar irradiance G and cell temperature T. The panel's electrical variables, namely PV voltage V_{pv} and PV current I_{pv}, are measured to calculate the instantaneous power. The hybrid controller receives G, T, V_{pv}, and I_{pv}. The ANN estimates the optimal voltage V_{ANN}, close to the voltage corresponding to the maximum power point. This estimate enables rapid repositioning of the operating point after a change in irradiance or temperature. A local P&O correction is then applied around the ANN reference. The final reference is defined as $V_{ref} = V_{ANN} + \Delta V_{PO}$, where ΔV_{PO} is a small voltage correction. The correction is bounded to avoid excessive excursions around the operating point estimated by the ANN. The voltage reference V_{ref} is compared with the measured voltage V_{pv}. The resulting error is processed by a PID controller, which generates the PWM duty cycle. This signal drives the buckconverter MOSFET and adjusts the apparent impedance seen by the PV panel. Thus, the ANN provides rapid repositioning toward the MPP region, while P&O performs fine adjustment around that region. This structure can reduce the search time observed with conventional P&O while retaining a local correction capability when the ANN estimate is inaccurate due to variations in operating conditions or model mismatch.

Hybrid controller principle: -

Hybrid operation has two complementary phases. After a detected change in G or T, Vref is immediately reset to V_{ANN} for 10 ms. P&O then refines V_{ref} every 5 ms with a 0.01 V step. The correction is bounded to ±1.5 V around V_{ANN}, and Vref is limited to 20–34 V. The ANN provides a fast global MPP estimate, whereas the hybrid P&O performs only a local search. Under nominal conditions, the hybrid and standalone ANN are expected to be very close. The expected benefit of hybrid P&O is mainly correction of ANN estimation errors. P&O performs local refinement around this point to reduce steady-state oscillations.

This combination addresses the individual limitations of each method: -

- slow tracking and oscillations for P&O;
- dependence on training quality and training-domain validity for the ANN [4], [9].

Switching Strategy: -

The transition between phases is triggered by $|G-G_{prev}| > 20$ W/m² or $|T-T_{pre}v| > 0.5$ °C. At each change, the P&O memory states are reset and the ANN temporarily takes control; P&O refinement starts only after the repositioning interval. Switching therefore does not rely on an unbounded power perturbation. It relies on changes in G and T available in the model, which makes the control logic reproducible. $|\Delta P/P|>\varepsilon$ the system is considered to be in a transient regime when a significant change in irradiance or temperature is detected, and the ANN is activated to rapidly reposition the operating point. Once the system approaches the MPP region, the P&O method takes over to refine the tracking and reduce oscillations. The system is close to the MPP, and the P&O method takes over to refine tracking and reduce oscillations. The threshold ε is selected empirically to ensure a speed–stability compromise; this tuning trade-off is commonly discussed for fixed-step and adaptive-step P&O methods [6], [7]. Simulation and results Monthly climate data from Ziguinchor are used for Buck-converter pre-sizing. They do not replace the dynamic profile used to compare the MPPT methods. Table 3 presents the monthly operating points used to estimate the L and C constraints. P_{max}, V_{mp}, and Imp are calculated for each (G,T) pair in Table 3 using the PV model. They are used to select standardized component values with sufficient margin for the most demanding operating conditions. Table 3 summarizes the monthly climate data and the Buck pre-sizing values.

Table 3: Climate Data and Buck Converter Pre-Sizing

Month	Irradiance G (W/m²)	Temperature (°C)	P_{max} (W)	V_{MP} (V)	I_{MP} (A)	L_{min} (µH)	C_{min}(µF)
January	756.28	28.6	186.7	28.88	6.513	130.3	40.5
February	803.05	30	197.5	28.68	6.873	119	42.9
March	880.38	31.5	215.4	28.39	7.58	103.4	46.7
April	859.88	32.4	209.7	28.28	7.42	103.9	45.5
May	701.14	32.74	170.3	28.38	6.00	130.5	37
June	591.62	31.28	143.6	28.45	5.05	156.9	31.2
July	517.54	29.02	125.9	28.65	4.42	185.6	27.3
August	497.01	28.18	120.8	28.68	4.21	194.5	26.2
September	613.89	29.09	150.4	28.74	5.25	157.9	32.6
October	664.30	29.79	162.8	28.61	5.69	142.5	35.3
November	799.22	30.93	195.8	28.58	6.85	117.9	42.5
December	745.87	29.87	183.3	28.68	6.39	128.2	39.8

Pre-sizing yields a maximum L_{min} value close to 195 µH and a maximum C_{min} value close to 47 µF. The selected values are L = 220 µH, C_1 = 220 µF, and C_2 = 470 µF. C1 decouples the PV generator, whereas C2 limits output ripple. The Buck converter supplies an equivalent 2.3 Ω resistive load at approximately 24 V. This choice validates MPPT operation and conversion losses; it does not model the electrochemical dynamics of a 24 V battery. Table 4 summarizes the final Buck-converter parameters used in the simulation.

Table 4: Buck Power Converter Specifications

Parameters	Value
Inductance L	220 µH
Input capacitor C1	220 µF
Output capacitor C2	470 µF
Switching frequency fs	20 kHz
Load resistance RL	2.3 Ω
Nominal output voltage	24 V
Discrete electrical time step	1 µs

Effect of temperature and irradiance on the maximum power of the PV panel:-
Figure 7 illustrates the dependence of Pmax on irradiance and temperature in the monthly data. This figure is a pre-sizing analysis rather than the dynamic MPPT comparison scenario.

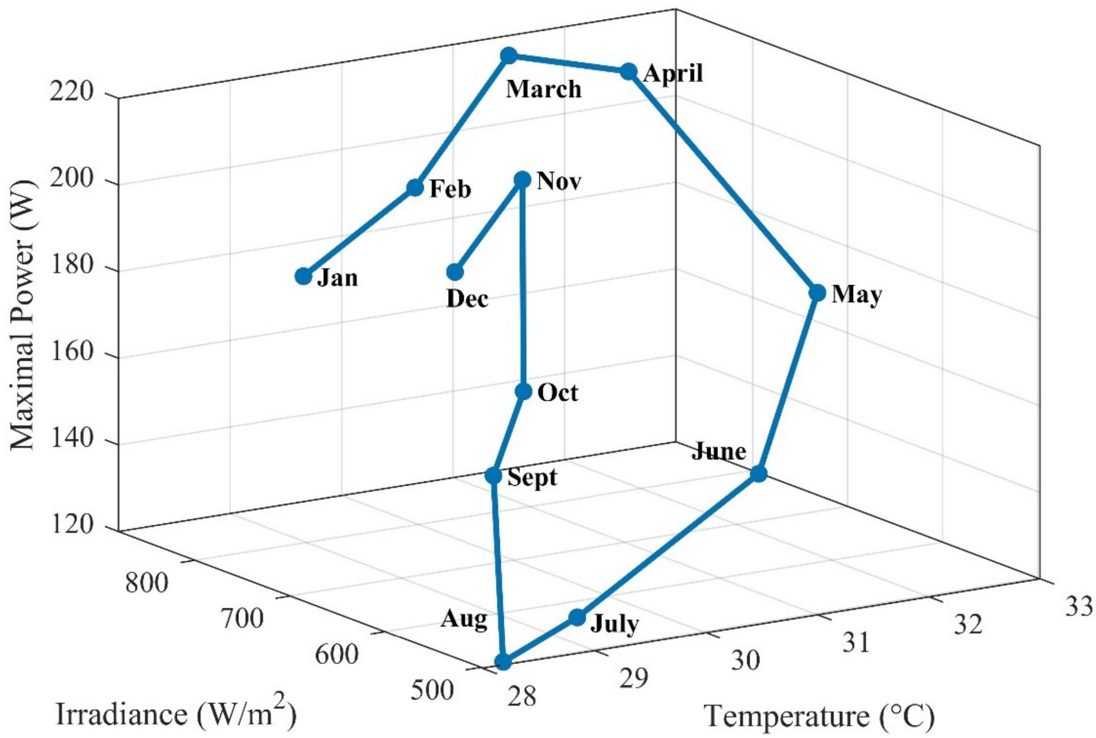

Figure 7. Maximum power as a function of temperature and irradiance

Table 3 confirms that irradiance is the dominant factor affecting maximum power over the range studied. Temperature mainly modifies the MPP voltage and makes a secondary contribution to P_{max} variation. The highest monthly value in this series occurs in March: G = 880.38 W/m², T = 31.5 °C, and P_{max} = 215.4 W. April is close, with P_{max} = 209.7 W. The thermal effect must not be confused with the irradiance effect: at equal irradiance, increasing T generally reduces Voc and shifts Vmp; in the monthly data, G and T vary simultaneously. From May to August, the decrease in mean irradiance explains most of the decrease in Pmax. For example, the minimum of the series occurs in August with G = 497.01 W/m² and P_{max} = 120.8 W. These climate data are useful for assessing seasonal potential and sizing the converter. The transient performance of the MPPT methods is evaluated separately using the G(t) profile defined below.

Comparison of MPPT: -
The dynamic comparison uses a total duration of 0.5 s and the following profile at T = 25 °C: 1000 W/m² (0 - 0.1 s), 600 W/m² (0.1 - 0.2 s), 800 W/m² (0.2 - 0.3 s), 400 W/m² (0.3 - 0.4 s), and 1000 W/m² (0.4 - 0.5 s). At 20 kHz, the simulation contains 10,000 PWM periods; each plateau contains 2,000 PWM periods and 100 conventional P&O updates.

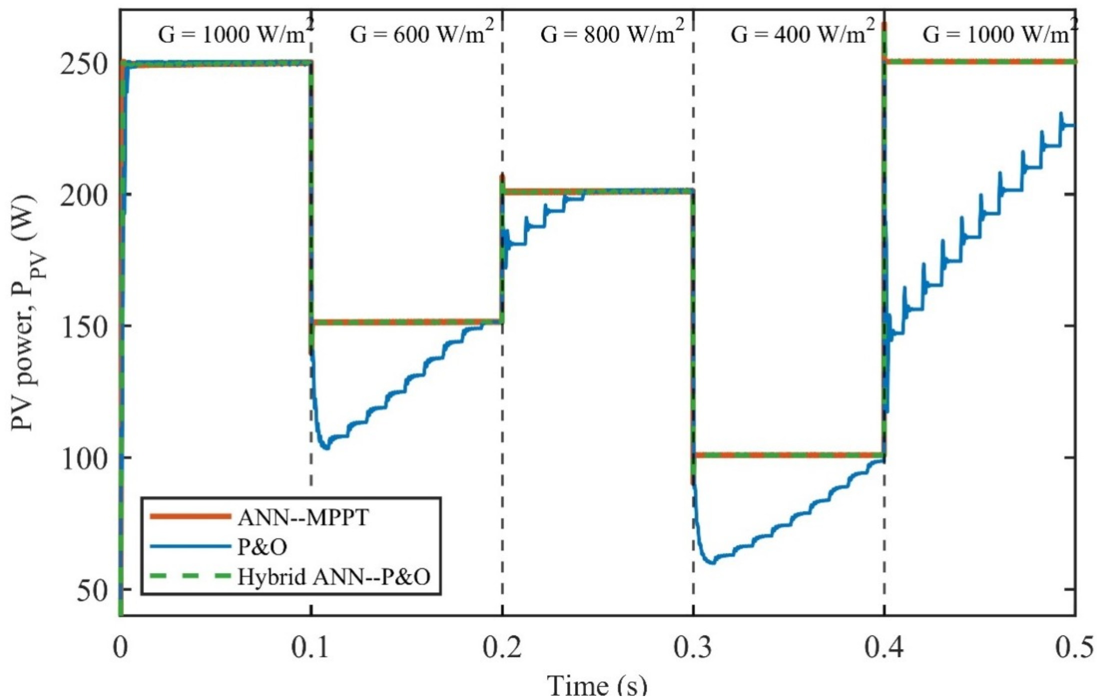

Figure 8: Dynamic performance comparison of MPPT algorithms

The performance indicators are defined separately as follows. Tracking accuracy is the instantaneous closeness of Ppv to the model-derived maximum power P_{MPP} and may be expressed as $100[1 - |P_{pv} - P_{MPP}|/P_{MPP}]$.
Tracking efficiency is an energy-based quantity, defined over an analysis interval $[t_1,t_2]$ as $\eta_{MPPT} = 100\int P_{pv}(t)dt/\int P_{MPP}(t)dt$.Power ripple is the steady-state peak-to-peak variation, $\Delta P_{pv} = P_{pv,\ max} - P_{pv,\ min}$, evaluated over the final portion of each irradiance plateau. Response time is the elapsed time after an irradiance transition until Ppv enters and remains within a ±2% band around P_{MPP}. These quantities are not interchangeable: a controller may have a high mean power while still exhibiting substantial ripple or a long settling time.

Table 5 compares the indicators extracted for standalone ANN and conventional P&O under the same dynamic profile. Table 5 presents the available results for standalone ANN, conventional P&O, and the hybrid ANN–P&O controller. The ANN reaches the reference within the resolution of the discrete model, and its filtered ripple ranges from 0.061 to 0.665 W over the steady-state windows. Conventional P&O exhibits substantially larger oscillations after some transitions and does not settle before the end of the final two windows. Efficiency values slightly above 100% result from discretization and the finite analysis window; they do not represent physical efficiency above 100%. This behavioral difference follows from the nature of the two methods: the ANN directly evaluates a trained function, yielding microsecond-scale response times, whereas P&O converges through successive $\Delta D = 0.002$ steps every millisecond, structurally linking its speed to the pair (ΔD, Ts,P&O). Although standalone ANN is already effective under nominal conditions, the specific benefit of P&O refinement is expected when the ANN estimate deviates from the real model, which the robustness test described in the conclusion is intended to quantify.

Literature-based interpretation: the degradation observed with conventional P&O after irradiance changes is qualitatively consistent with the analyses of Femia et al. [6], which link the perturbation step to oscillations and convergence time, and with the experimental comparisons of Hohm and Ropp [7]. The results should not be compared numerically on a one-to-one basis with those studies because the PV module, converter, switching frequency, sampling interval, and response-time indicators differ. The relevant correlation is therefore a trend-level consistency: P&O exhibits a speed–ripple trade-off, whereas an ANN estimate can rapidly reposition the reference but must be validated outside its training domain [4], [9].

Table 5: Dynamic Indicators for Standalone ANN, Conventional P&O, and Hybrid ANN–P&O

Transition (W/m²)	ANN mean P_{pv} (W)	ANN ripple (W)	ANN response	P&O mean P_{pv}(W)	P&O ripple (W)	P&O response	Hybrid mean P_{pv} (W)	Hybrid ripple (W)	Hybrid response
1000→600	151.49	0.414	≤ 3 µs	141.73	22.17	82.80 ms	151.48	0.631	≤ 2 µs
600→800	201.06	0.665	≤ 2 µs	201.29	0.800	32.57 ms	201.09	0.850	≤ 2 µs
800→400	100.95	0.061	≤ 1 µs	86.58	23.94	> 100 ms	100.92	0.182	≤ 1 µs
400→1000	250.25	0.225	≤ 2 µs	206.72	44.23	> 100 ms	250.25	0.308	≤ 2 µs

Conclusion: -

This article presented the modeling of a 250.27 W PV module, a Buck converter, and three MPPT strategies: conventional P&O, ANN, and hybrid ANN–P&O. The hybrid controller is formulated around a voltage reference, making it consistent with the Vref–PID–PWM loop and avoiding direct mixing of duty cycles. Nominal simulations show that conventional P&O is slower and more oscillatory than ANN. The hybrid controller nearly overlaps with ANN in the nominal model because the ANN was trained on that same model. This observation validates that the hybrid control does not degrade nominal operation, but it does not demonstrate that it systematically outperforms standalone ANN. The study therefore establishes the methodological framework for the hybrid approach; its specific added value remains to be demonstrated by the defined robustness test, in which the simulated PV model is altered (Rs = 0.352 Ω, i.e., +20%, and Rsh = 97.41 Ω, i.e., −20%) without retraining the ANN, while keeping the same G(t) profile, converter, and P&O parameters. This test will enable comparison of standalone ANN, P&O, and hybrid control when the ANN estimate is imperfect and will determine whether the P&O refinement provides a specific benefit.

References: -

[1] M. G. Villalva, J. R. Gazoli and E. R. Filho, “Comprehensive Approach to Modeling and Simulation of Photovoltaic Arrays,” IEEE Transactions on Power Electronics, vol. 24, no. 5, pp. 1198–1208, 2009. DOI: 10.1109/TPEL.2009.2013862.
[2] W. De Soto, S. A. Klein and W. A. Beckman, “Improvement and Validation of a Model for Photovoltaic Array Performance,” Solar Energy, vol. 80, no. 1, pp. 78–88, 2006. DOI: 10.1016/j.solener.2005.06.010.
[3] T. Esram and P. L. Chapman, “Comparison of Photovoltaic Array Maximum Power Point Tracking Techniques,” IEEE Transactions on Energy Conversion, vol. 22, no. 2, pp. 439–449, 2007. DOI: 10.1109/TEC.2006.874230.
[4] A. Mellit and S. A. Kalogirou, “Artificial Intelligence Techniques for Photovoltaic Applications: A Review,” Progress in Energy and Combustion Science, vol. 34, no. 5, pp. 574–632, 2008. DOI: 10.1016/j.pecs.2008.01.001.
[5] A. R. Reisi, M. H. Moradi and S. Jamasb, “Classification and Comparison of Maximum Power Point Tracking Techniques for Photovoltaic System: A Review,” Renewable and Sustainable Energy Reviews, vol. 19, pp. 433–443, 2013. DOI: 10.1016/j.rser.2012.11.052.
[6] N. Femia, G. Petrone, G. Spagnuolo and M. Vitelli, “Optimization of Perturb and Observe Maximum Power Point Tracking Method,” IEEE Transactions on Power Electronics, vol. 20, no. 4, pp. 963–973, 2005. DOI: 10.1109/TPEL.2005.850975.
[7] D. P. Hohm and M. E. Ropp, “Comparative Study of Maximum Power Point Tracking Algorithms,” Progress in Photovoltaics: Research and Applications, vol. 11, no. 1, pp. 47–62, 2003. DOI: 10.1002/pip.459.
[8] M. T. Mitsuya and A. A. de Moura Meneses, “Efficiency of Hybrid MPPT Techniques Based on ANN and PSO for Photovoltaic Systems under Partially Shading Conditions,” American Journal of Engineering and Applied Sciences, vol. 12, no. 4, pp. 460–471, 2019. DOI: 10.3844/ajeassp.2019.460.471.
[9] M. Y. Worku, M. A. Hassan, L. S. Maraaba, M. Shafiullah, M. R. Elkadeem, M. I. Hossain and M. A. Abido, “A Comprehensive Review of Recent Maximum Power Point Tracking Techniques for Photovoltaic Systems under Partial Shading,” Sustainability, vol. 15, no. 14, art. 11132, 2023. DOI: 10.3390/su151411132.
[10] M. A. G. de Brito, L. Galotto, L. P. Sampaio, G. de Azevedo e Melo and C. A. Canesin, “Evaluation of the Main MPPT Techniques for Photovoltaic Applications,” IEEE Transactions on Industrial Electronics, vol. 60, no. 3, pp. 1156–1167, 2013. DOI: 10.1109/TIE.2012.2198036.

[11] M. T. Hussain, A. Sarwar, M. Tariq, S. Urooj, A. BaQais and M. A. Hossain, “An Evaluation of ANN Algorithm Performance for MPPT Energy Harvesting in Solar PV Systems,” Sustainability, vol. 15, no. 14, art. 11144, 2023. DOI: 10.3390/su151411144.
[12] M. Z. El Masry, A. Mohammed, F. Amer and R. Mubarak, “New Hybrid MPPT Technique Including Artificial Intelligence and Traditional Techniques for Extracting the Global Maximum Power from Partially Shaded PV Systems,” Sustainability, vol. 15, no. 14, art. 10884, 2023. DOI: 10.3390/su151410884.
[13] B. Cruz, L. Ricalde, R. Quintal-Palomo, A. Bassam and R. I. Rico-Camacho, “Hybrid Artificial Neural Network and Perturb & Observe Strategy for Adaptive Maximum Power Point Tracking in Partially Shaded Photovoltaic Systems,” Energies, vol. 18, no. 19, art. 5053, 2025. DOI: 10.3390/en18195053.